Segmentation of Melanoma and Non-Melanoma Skin Images Using Integrated k-Means Clustering and Local Gaussian Distribution Fitting

Noor Badshah[*], Nasru Minallah[**], Muniba Ashfaq[**], Muhammad Abeer Irfan[**], ∗ Asif Ahmad[*], Mahmood Ul Hassan[*], Zain Anwer Memon [***]

[*] Department of Basic Sciences, University of Engineering and Technology Peshawar, 25000, Pakistan.
[**]Department of Computer Systems Engineering, University of Engineering and Technology Peshawar, 25000, Pakistan.
[***]Department of Electronics Engineering, University of Sindh, Jamshoro, 76080, Pakistan

Abstract- This paper introduces a novel methodology for precise segmentation of melanoma and non-melanoma skin images. Initially, a Region of Interest (ROI) encompassing the lesion is extracted from the input image. Subsequently, the image undergoes preliminary segmentation via k-means clustering to isolate the lesion region, followed by refinement using morphological operations. The resulting segmentation serves as the basis for initializing the contour in the application of the Local Gaussian Distribution Fitting (LGDF) energy model, a well-established method for segmenting skin images. Extensive evaluation on a publicly available dataset comprising both melanoma and non-melanoma skin images demonstrates the superior performance of our proposed approach in terms of segmentation iterations, accuracy, and computational time. Our method offers a promising tool for aiding clinicians in the early diagnosis and treatment planning of skin cancer.

Index Terms- Melanoma, Non-melanoma, Region of Interest, k-mean Clustering, Morphological Operation, and Gaussian Distribution.

I. INTRODUCTION

The The predominant forms of cancer in the modern world are skin cancers, specifically melanoma and non-melanoma. These neoplasms have elevated the global prevalence of cutaneous malignancies [1]. According to data from the American Institute for Cancer Research in 2018, approximately 22 percent of skin cancer cases were classified as melanoma, while the remaining 78 percent were classified as non-melanoma. The most prevalent non-melanoma tumours are basal cell carcinoma and squamous cell carcinoma. In 2018, the global incidence of melanoma reached 300,000 new cases, positioning it as the 19th most prevalent form of cancer among both males and females. Non-melanoma ranks as the fifth most prevalent form of cancer in both males and females, with a reported incidence exceeding one million cases [2]. The increased prevalence rates can be attributed to various factors, including exposure to UV radiation [3], shifts in clothing patterns, heightened outdoor activities, the depletion of the ozone layer, an extended lifespan, genetic predisposition, and the induction of immune system suppression [4]. According to estimates, approximately 20 individuals in the United States succumb to melanoma on a daily basis. The projected number of deaths caused by melanoma in 2019 is around 7230, with 4745 being males and 2485 being women [2]. Indicators of skin cancer include any alteration in the shape, colour, or size of a bruise, an unhealing sore on the skin, or abnormal growth of the skin. The timely identification of the lesion has the potential to enhance the likelihood of successful treatment and significantly decrease both illness and death rates.

During the initial phases of skin cancer, the manual diagnosis relies on the availability of proficient physicians equipped with appropriate medical equipment. In numerous instances, the absence of specialized medical practitioners and adequate healthcare infrastructure hinders the timely detection of skin cancer. In the field of dermoscopy, the detection of skin cancer is facilitated through the utilization of an automated computer-aided diagnosis (CAD) system [5]. Automated computer-aided design (CAD) has been employed within the medical domain for over a decade. Skin lesions are being classified using a computer-aided design (CAD) system that employs image processing and machine learning methods. Segmentation holds greater significance in CAD. Segmentation in computer-aided design (CAD) involves the division of a dermoscopy image into two distinct regions: the lesion region and the unaffected region. The outcomes of the diagnostic system are significantly influenced by the level of segmentation executed.

The literature has offered several methodologies for the segmentation of cutaneous lesions [6], [7], [8], [9]. There are three primary classifications for segmentation techniques: clustering-based, threshold-based, and active contours. The statistical region merging (SRM) algorithm, proposed by Emre Celebi et al. [10], is founded on the principles of region growth and region merging. The approach developed by the researchers demonstrated superior performance compared to four existing automatic methods, namely orientation-sensitive fuzzy c-means, mean shift clustering, the tumour extraction algorithm, and the modified JSEG method.

The authors [11] suggested employing JSEG algorithms for the purpose of identifying the boundaries of skin lesion images [12]. The algorithm's primary function is to partition the segmentation process into two distinct components: colour quantization and

spatial segmentation. A different method for segmenting skin lesions is introduced in [13], which utilizes a histogram-based clustering estimation (HBCE) algorithm and neuromorphic c-means clustering methods (NCM) for skin lesion detection. The approach under consideration involves the mapping of the picture into the neuromorphic domain. Subsequently, an NCM algorithm is employed to group the pixels. The number of clusters is then estimated using the HBCE algorithm. Finally, lesion segmentation is performed based on the intensity and morphological properties of the lesion. The authors in [6] have suggested a set of thresholding approaches to detect lesion borders in dermoscopy images. The authors in [14] have suggested techniques for distinguishing between skin and non-skin colors by employing a piecewise linear decision boundary. The proposed methods establish predetermined skin thresholds within a specified colour space. The authors of [8] propose an automated approach for the segmentation of photos depicting skin cancer. This approach involves the conversion of an RGB image into an intensity image, followed by the application of intensity thresholding to effectively segment the image. In addition, the segmentation process is enhanced through the utilization of double thresholding. Thresholding is a straightforward and efficient method for segmentation. The segmentation of photos exhibiting high contrast yields satisfactory outcomes. Nevertheless, this approach is also ineffective due to its uneven outcomes, since certain photos exhibit a lack of distinction between the skin and lesion or a diminished contrast.

The active contour algorithm is a segmentation approach. Active contour methods, sometimes referred to as "snakes," are extensively employed in the field of picture segmentation [15], [16], [17], and [18]. There are two primary classifications for active contours: edge-based methods [19] and region-based methods [20]. The use of edge information [15], [18] is employed in the edge-based method, whereas the region-based method relies on region characteristics and directs the active contour towards the boundary of an object for segmentation [21], [22]. Active contours are a set of procedures that commence their operation by establishing an initial contour around the region of interest (ROI). This initial contour then undergoes movement and cessation at the boundary of the item that is to be segmented. The aforementioned approaches incorporate parameters that regulate the level of contour smoothness and facilitate its convergence towards the central region of interest (ROI). Although edge-based active contours have the benefit of effectively managing intricate shapes, their utilization is hindered by the complexity of their parameters. Active contours based on edges are appropriate for detecting lesions [15], [18]. However, their efficiency is diminished in cases where the borders of an image exhibit smoothness. Likewise, region-based techniques exhibit limitations such as the potential for fluctuating values of

The parameters vary across various images, necessitating a higher number of iterations. Additionally, the size and coordinates of the starting contour are altered by each image, rendering them susceptible to initialization and rendering the segmentation process laborious. The authors Wang et al. have introduced an active contour driven by local Gaussian distribution fitting energy (LGDF) [23], which encounters similar challenges. In contrast to existing region-based active contour models [20], [21], LGDF possesses a distinct advantage due to the incorporation of local intensity means and variances as spatially variable functions. This enables the model to effectively differentiate regions characterized by similar means but varying variances.

In the last decade, various neural networks within the field of deep learning have been suggested for the purpose of segmenting medical images, demonstrating exceptional performance. The majority of networks proposed for the task are derived from U-Net [24], a neural network specifically designed for the purpose of biomedical image segmentation. The implementation of these networks incurs significant expenses, mostly because to the high costs associated with big data and sophisticated equipment, rendering them inaccessible to the general population.

This study introduces a methodology that addresses the aforementioned limitations of the LGDF model, namely equation (3). In the course of conducting studies on medical images, it was observed that the LGDF model had more promising results compared to other active contour-based models [20], [18]. Additionally, it has been observed that the outcomes of the LGDF model can be significantly enhanced with the provision of appropriate initial shape. In this research, we present a methodology that offers an automated initialization process for the model. In order to achieve this objective, we have implemented several pre-processing approaches.

The subsequent section of this work is structured as follows: Section 2 of the paper focuses on the relevant literature. Section 3 introduces the proposed methodology. Section 4 provides an explanation of the measurement quantities employed to obtain the results. Section 5 offers a comprehensive analysis of the experimental findings. Section 5.1 delves into the origin and characteristics of the data set utilized in the experiment. Section 6 serves as a dedicated section for further deliberation. Lastly, section 7 concludes the paper with a concluding note.

II. IDENTIFY, RESEARCH AND COLLECT IDEA

The utilization of either pre-processing, post-processing, or a combination of both techniques has the potential to enhance the segmentation of skin images. [25] utilizes both methodologies to partition photos that include skin lesions. In the present study, the researchers have employed dermoscopy pictures with a resolution of 8 bits. Initially, the active contour was chosen during the pre-processing phase, serving the purpose of extracting the region of interest. The subsequent phase of the process is colour improvement, which is subsequently followed by grey thresholding, hair removal, and the elimination of dark corners from the image. The final stage of the pre-processing procedure involves using Cohen-Daubechies-Feauveau biorthogonal wavelets to segment the image [26]. Finally, during the post-processing stage, morphological techniques were implemented to obtain the ultimate segmented outcome. The aforementioned procedures are utilized to address potential voids within the segmented lesion area. The methodology that was proposed demonstrated an average true detection rate (ATDR) of 93% and an average false positive rate (AFPR) of 5.43%. This study utilizes dermoscopy images from a pH data set to conduct the experiment.

The comparison between two segmentation techniques, namely active contour and fuzzy clustering based on region growth

(FCR), was conducted by the authors in reference [27]. Prior to utilizing the input images for skin image segmentation, they undergo pre-processing. The pre-processing procedures involve converting RGB to grayscale and then selecting only the blue colour channel. Additionally, image filtering is performed to remove hair and smooth the image. Furthermore, dark spots in the corners of the photos are detected. The segmentation results of the two algorithms were compared, revealing that the FCR and active approaches achieved high accuracy rates of 97.6% and 96.4% respectively.

A study conducted by [28] presents a comparison of the outcomes of six segmentation methods on melanoma photos obtained from the clinical database of Hospital Pedro Hispano, Mousinho's, Portugal. Prior to the application of the procedures, pre-processing techniques have been employed. Segmentation. During the initial phase of data processing, a morphological closure filter was employed to eliminate characteristics associated with black hair. Subsequently, the dark corners present in the photos were eliminated by gray-level thresholding utilizing Otsu's method. Subsequently, the binary components associated with the terminal points of the images were removed. A comparative analysis was conducted on six segmentation methods, namely gradient vector flow (GVF), the level set method of Chan et al. (C-LS), adaptive thresholding (AT), adaptive snakes (AS), EM level set (EM-LS), and fuzzy-based split and merge algorithms (FBSM). The findings indicated that the AS and EM-LS methods exhibited superior performance in terms of true detection rate (TDR), with values of 95.47% and 95.20% respectively. A TDR of 93.67% was attained by the FBSM. The researchers have reached the conclusion that the AS and EM-LS techniques exhibit more robustness and use in the segmentation of lesions within a computer-aided diagnosis system.

In the study conducted by [29], a rapid and fully automated technique is introduced for the purpose of segmenting skin pictures that contain lesions. The method under consideration is divided into four distinct stages: artefact elimination and picture standardization, skin identification, lesion delineation, and consolidation. The authors offer a strategy called HBCENCM, which utilizes the histogram-based clustering estimation (HBCE) algorithm. This algorithm is necessary for determining the optimal number of clusters in the neuromorphic c-means clustering (NCM) method [13]. The detection of a skin lesion relies on the assessment of its intensity and morphological characteristics. Their average accuracy on the ISIC 2016 data set is 96.3%.

Sectioning and categorization are performed in reference [30]. The present study is structured into four distinct phases. Initially, there was the application of filtering and contrast enhancement techniques. Additionally, an assessment is conducted on segmentation, thresholding, and statistical features in order to identify the presence of the lesion. Entropy and bi-fold are employed in the third step to compute feature extraction and asymmetry. The ultimate phase entails the process of classification. The proposed methodology is implemented on a dataset consisting of 200 dermoscopy images. The obtained outcomes demonstrate an average accuracy of 90%, sensitivity of 85%, and specificity of 92.22%. The authors in reference [31] have examined two distinct techniques designed for the identification of melanomas in skin pictures. The initial approach employs global techniques to categorize skin photos, while the subsequent approach utilizes local characteristics and a bag-of-features classifier.

After performing pre-processing techniques such as contrast enhancement, anisotropic diffusion, and hair removal using a morphological filter, the segmentation process in [7] involves the utilization of geodesic active contours. In a similar vein, [32] presents a geodesic active contour (GAC) technique that draws inspiration from biology to segment lesions in skin pictures. In reference [18], gradient vector flow (GVF) snakes are also employed. This system is designed to autonomously identify the boundaries of skin lesions in dermoscopy images. This approach incorporates an automated initiation technique to achieve complete automation of the process.

III. PROPOSED WORK

In this section, we elucidate our methodology, which enhances the efficiency and resilience of the LGDF model, as represented by equation (3), during the initialization process. Several pre-processing approaches were employed for this objective. The workflow, as depicted in Figure 4, is outlined as follows.

A. ROI Extraction

We transform an RGB skin picture with lesions to grayscale first. Draw a rectangular or square mask around the lesion to extract the region of interest. The mask extracts the lesion and excludes the rest. Extra regions are removed to avoid illumination effects that could compromise segmentation. MATLAB (R2017b) built-in imcrop tool extracts ROI. Figure 1 shows ROI extraction cropping the rectangular figure. The clipped image is utilised for rough segmentation.

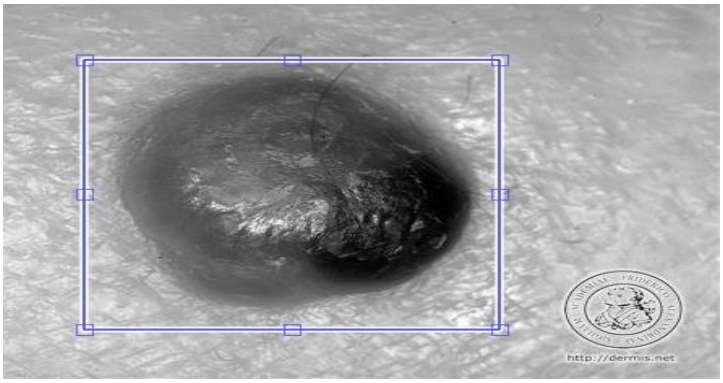

Figure 1: Extraction of Region of Interest (ROI) shown in the blue bounding box.

B. Segmentation

After extracting the ROI from a picture, we use the k-mean clustering approach to rough segment the ROI lesion. K-means clustering segments images unsupervised [33, 34]. K-mean clustering segments images into classes by k distinct clusters. We start with k = 2 and discover cluster centers. Each pixel in the region is classed by Euclidean distance from the cluster center [35]. P (x, y) is a ROI pixel and ck is the cluster center. Calculate the distance as follows.

$$d = ||P(x,y) - c_k||$$

After classifying all pixels, we recalculate the cluster centroid until it meets the tolerance or error value. Recalculation uses this equation.

$$c_k = \frac{1}{k} \sum_{y \epsilon C_k} \sum_{x \epsilon C_k} P(x,y), \qquad k = 1,2$$

In order to obtain a segmented image, a classified pixel is first reshaped into an image format depicted in Figure 2.

Figure 2: Morphological Operations and K-means clustering results.

C. Morphological Operation

Figure 2 shows that k-mean segmentation leaves holes in the approximately segmented region. We fill the voids with repeated morphological processes. These actions use three built-in MATLAB (R2017b) commands: imclose, imfill, and strel. Our method fills the gaps (background pixels) in the segmented ROI with one imfill cycle [36]. We fill huge gaps with a 10-pixel disc structural element and the strel command [37]. This structure element closes morphological activities in imclose. Dilation followed by erosion with the same structuring element creates a closed image. Another imfill cycle covers further flaws; Figure 2 displays morphological procedures.

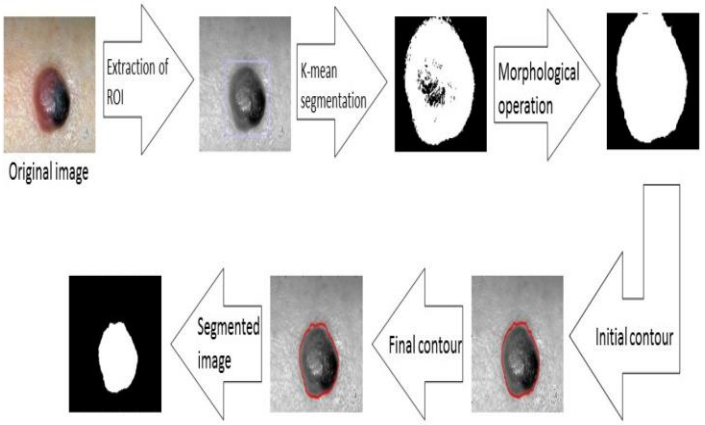

Figure 3. Developed Methodology flowchart.

Boundary extraction from the morphological operation image is utilized to create the LGDF model's initial contour, explained next. A morphologically segmented image instead of a triangle, circle, rectangle, or square is used to start the LGDF.

D. LGDF Model

The Wang et al. [23] active contour model uses local Gaussian distribution fitting (LGDF) energy to segment the skin lesion. The model uses more complicated statistical properties of local intensities to characterize the distribution of local intensity information via neighborhood partitioning. LGDF's energy function is

$$\begin{aligned} E^{LGDF}(\phi, p_{1,x}, p_{2,x}) &= \mu \int_\Omega \frac{1}{2}(|\nabla\phi| - 1)^2 \, dx + \nu \int_\Omega \delta_\varepsilon(\phi)|\nabla\phi| dx \\ &- \lambda_1 \int_\Omega \left(\int_{\Omega_1} \omega(x-y) \log p_{1,x}(I(y)) H_\epsilon(\phi(y)) dy \right) dx \\ &- \lambda_2 \int_\Omega \left(\int_{\Omega_2} \omega(x-y) \log p_{2,x}(I(y)) [1 - H_\epsilon(\phi(y))] dy \right) dx \end{aligned}$$

In the preceding equation, Ω1 and Ω2 represent regions inside and outside, respectively, the zero-level set of φ. Here, a local circle region is taken by using x as a pixel point, and the region is further divided into N number of sub-regions, $\{\Omega_i\}_{i=1}^{N}$, which are disjoint [38]. In the ith sub-region, a pixel pointy is taken with the intensity I(y), and its posteriori probability is used, which is denoted by pi,x (I(y)).ω(x − y) is a weighting function that relies on the length of the space between the two points, x, and y.
Regularization terms are the first two terms, along with the non-negative terms μ and ν. The first is called the "distance regularizing term", which is used to ensure stable evolution of the level-set function φ [39]. The second term is known as the length regularizing term, which regularizes the zero-level contour of φ. The coefficients λ1 and λ2 are positive constants that are used for controlling movement of the contour. If the contour must contract towards its center, then λ1 is assigned a greater value than λ2, and in the other case, λ2 is taken as greater. The posteriori probability and weighting function are given by:

$$\omega(y-x)=\frac{1}{a}\exp\left(-\frac{|(y-x)|^2}{2\sigma^2}\right)$$

$$p_{i,x}=\frac{1}{\sqrt{2\pi}\sigma_i(x)}\exp\left(-\frac{u_i(x)-I(y)}{2\sigma_i^2(x)}\right),i=1,2.$$

where ui(x) represents local intensity means and σi(x) represents standard deviations. a is used as a constant in such a way that $\int \omega(d) = 1$. The d represents the distance between x and y, and σ > 0 is a scaler parameter. The value of the weighting function becomes zero if d is greater than the radius of the neighborhood around the pixel point x. A smoothing function HE is typically used as an approximation for the Heaviside function H, which is denoted as:

$$H_\epsilon(x)=\frac{1}{2}\left[1+\frac{2}{\pi}\arctan\left(\frac{x}{\epsilon}\right)\right]$$

The derivative of the smooth function, H_ϵ, is the smoothed Dirac delta function, given as:

$$\delta_\epsilon(x)=H_\epsilon^{'}(x)=\frac{1}{\pi}\frac{\epsilon}{\epsilon^2+x^2}$$

The following Euler-Lagrange equations are satisfied by the parameters ui and σ2, which minimize the energy functional, Eq. (3):

$$\int \omega(y-x)(u_i(x)-I(y))M_{i,\epsilon}(\phi(y))dy=0$$

$$\int w(y-x)\left(\sigma_i(x)^2-(u_i(x)-I(y))^2\right)M_{i,\epsilon}(\phi(y))dy=0$$

$$u_i(x)=\frac{\int \omega(y-x)I(y)M_{i,\epsilon}(\phi(y))dy}{\int \omega(y-x)M_{i,\epsilon}(\phi(y))dy}$$

$$\sigma_i(x)^2=\frac{\int \omega(y-x)(u_i(x)-I(y))^2M_{i,\epsilon}(\phi(y))dy}{\int \omega(y-x)M_{i,\epsilon}(\phi(y))dy}$$

$$\frac{\partial\phi}{\partial t}=-\delta_\epsilon(\phi)(e_1-e_2)+\nu\delta_\epsilon(\phi)\,\mathrm{div}\left(\frac{\nabla\phi}{|\nabla\phi|}\right)+\mu\left(\nabla^2\phi-\left|\mathrm{div}\left(\frac{\nabla\phi}{|\nabla\phi|}\right)\right|\right)$$

These two, Eq (10) and Eq (11), are used for energy functional minimization with fixed ϕ. The gradient descent flow equation for minimization of the energy function with respect to ϕ is [40]

$$e_1(x)=\int_\Omega \omega(y-x)\left[\log(\sigma_1(y))+\frac{(u_1(y)-I(x))^2}{2\sigma_1(y\quad)^2}\right]dy$$

$$e_2(x)=\int_\Omega \omega(y-x)\left[\log(\sigma_2(y))+\frac{(u_2(y)-I(x))^2}{2\sigma_2(y)^2}\right]dy.$$

The Dice similarity coefficient (DSC) and Jaccard Index are used for comparison. This statistic, known as the Sorensen Dice coefficient [41], measures the similarity and difference of two objects. The initial purpose was to compare two discrete data sets; later, it was used to compare ground truth and segmented images in image processing. The equation (16) for DSC is two times the intersection of the segmented picture and ground truth over the sum of their cardinalities. Jaccard Similarity coefficient (JI), established by Jaccard Paul [42], measures variety and similarity between ground truth and segmented picture. The intersection of the objects over their union yields the equation (15) for JI. If SI is the segmented image and GT is the ground truth, JI and DSC are:

$$JI=\frac{S_I\cap G_T}{S_I\cup G_T}$$

$$DSC=\frac{2*|S_I\cap G_T|}{|S_I|+|G_T|}$$

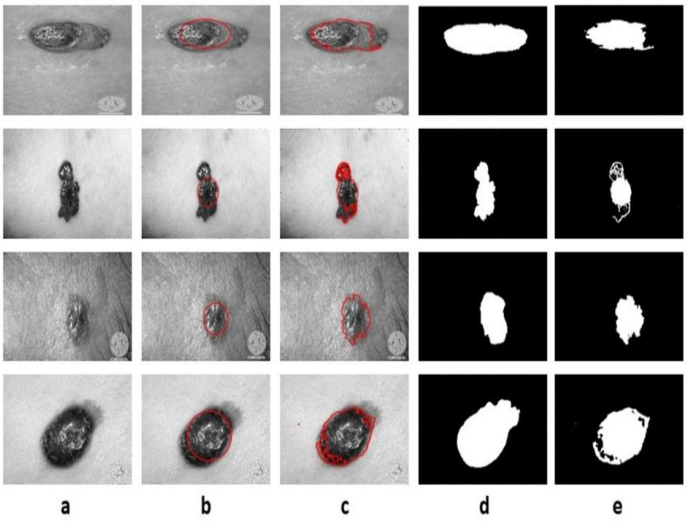

Figure 4: Results of LGDF on melanoma skin images from I/P image to segmentation.

Algorithm 1 Algorithm of the proposed method: Steps to be followed for implementation of our proposed method.
Data: Skin image.
Result: Segmented image.
Step I: Convert RGB image to gray.
Step II: Extract ROI from the image using imcrop command.
Step III: Apply k-mean segmentation using equations (1) and (2).
Step IV: Apply morphological operations using matlab commands: imfill, imclose and strel of radius 10 and disk shape.
Step V: Extract boundary of the segmented lesion finding edges with find command. Step VI: Put the extracted boundary as an initial contour for equation (3) on the image. Step VII: Initialize the level set function φ after setting values of parameters: σ, λ1, λ2, μ, and ν.
Step VIII: Using equation (10), (11) and (12) update ui(x), σi(x) and φ.
Step IX: Get the segmented image

IV. Experimental Result

We compare our results to the LGDF and LBF, local binary fitting model [43], which were applied to the identical images, as shown in Figures 6 and 7. Image IDs in Table 2 were randomly selected from the data set with ground facts. We kept the LGDF (3) settings and iterations the same for all trials utilising our technique. Using $\sigma = 3$, $\lambda 1 = \lambda 2 = 1.0$, $\mu = 1$, and $v = 0.0005 * 255 * 255$, we fixed 150 iterations. Melanoma pictures had average JI and DSC values of 0.9018 and 0.9475 in Eqs 15 and 16. Table 1 shows average non-melanoma picture JI = 0.9093 and DSC = 0.9255. We also noted the standard deviation values of each image from the mean JI and DSC values for melanoma and non-melanoma photos. We found standard deviation values of 0.047 and 0.0375 for non-melanoma images and standard values of 0.043 and 0.0306 for melanoma images from JI and DSC mean values. To achieve optimal results for LGDF and LBF, we used different iterations for each image: $\sigma = 3$, $\lambda 1 = 1.03$, $\lambda 2 = 1.0$, $\mu = 1$, and $v = 0.0005*255*255$ for LGDF, and $\sigma = 3$, $\lambda 1 = 1.0$, $\lambda 2 = 1.5$, $\beta = 1$, and $v = 0.005 * 255 * 255$ for LBF experiments. Table 1. Average JI and DSC results on melanoma and non-melanoma pictures using LGDF and LBF models. Table 2: The first and third rows reveal our paper values. Second and fifth rows show melanoma image identification numbers (IDMI), whereas third and last rows show non-melanoma image identification numbers (IDNMI).

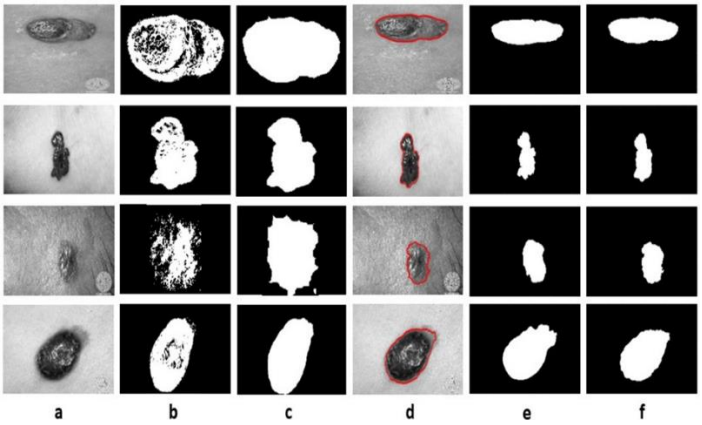

Figure 7: Results of our method on melanoma skin images, where column: (a) input images (b) results of k-mean clustering (c) results of morphological operations (d) final contours (e) ground-truth and (f) segmentation results.

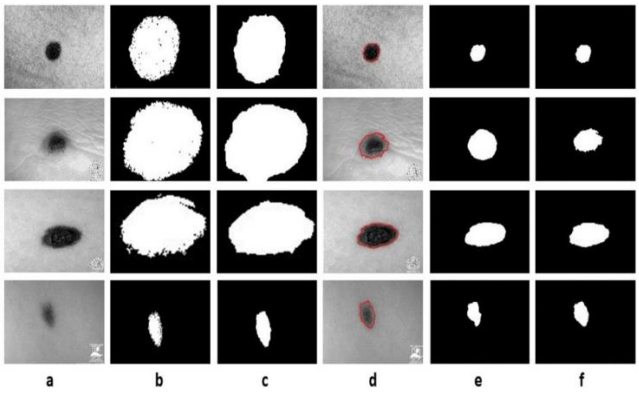

Figure 7: Results of our method on non-melanoma skin images, where column: (a) input images (b) results of k-mean clustering (c) results of morphological operations (d) final contours (e) ground-truth and (f) segmentation results.

Table 1: Comparison of results of the proposed approach with LGDF and LBF model.

	Melanoma			
	JI	DSC	Iterations	Time(sec)
Our Method	0.9018	0.9475	150	47.25
LGDF	0.7564	0.8559	2070	742.33
LBF	0.5714	0.7208	320	83.88
	Non-melanoma			
	JI	DSC	Iterations	Time(sec)
Our Method	0.9093	0.9255	150	87.22
LGDF	0.7274	0.8331	1000	363.05
LBF	0.4156	0.5444	300	778.4

Table 2: Our paper values are in the first and third rows of the table. Second and fifth rows show melanoma image identification numbers (IDMI), whereas third and last rows show non-melanoma image identification numbers (IDNMI).

Images	1	2	3	4
IDMI	NM1	SSM21	SSM57	LMM5
IDNMI	4	46	D41	34
Images	9	10	11	12
IDMI	SSM1	NM5	SSM14	NM61
IDNMI	23	10	D33	D11
Images	5	6	7	8
IDMI	AMM1	NM2	LMM9	NM4
IDNMI	41	D24	D30	29
Images	13	14	15	
IDMI	SSM31	LMM9	NM83	
IDNMI	25	D54	D16	

Compared to the LGDF and LBF, our initialization method is simple, fast, and resilient. Application on any skin picture requires one click after selecting the ROI. Comparisons demonstrate that our technique outperforms LGDF and LBF models. Comparisons are graphed below.

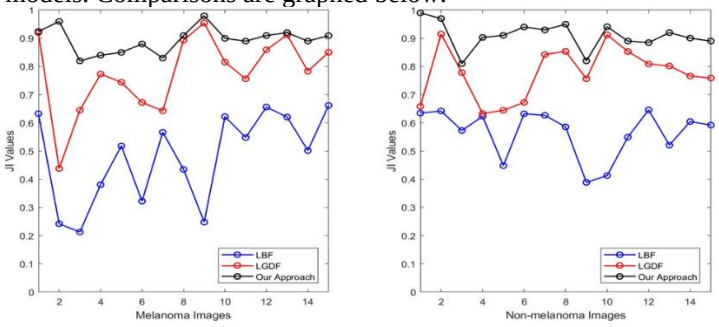

Figure 8: The LGDF and LBF JI values are graphed. Right compares fifteen non-melanoma photos, left compares fifteen melanoma images.

Dataset: The photographs are from DermIS 2 and DermQuest 3, which comprise melanoma and non-melanoma skin scans. Ground truth images of 89 melanoma and 26 non-melanoma are in the DermIS. DermQuest has 76 melanoma and 61 non-melanoma pictures and ground truths. Visit https://uwaterloo.ca/vision-image-processing-lab/research-demos/ skin-cancer-detection to view the database.

V. DISCUSSION

We developed a semi-automatic approach to segregate melanoma and non-melanoma skin lesions. The method accelerates the sluggish process of active contours with unknown regular size and position of the initial contour and the number of iterations needed to get the final contour. Figures 4(b) and 5(b) show that the first contour shape and size vary depending on the skin lesion structure. LGDF and LBF models have various iterations for each image. Table 1 shows that both techniques have more iterations than the suggested methodology, which is constant and less for each image.

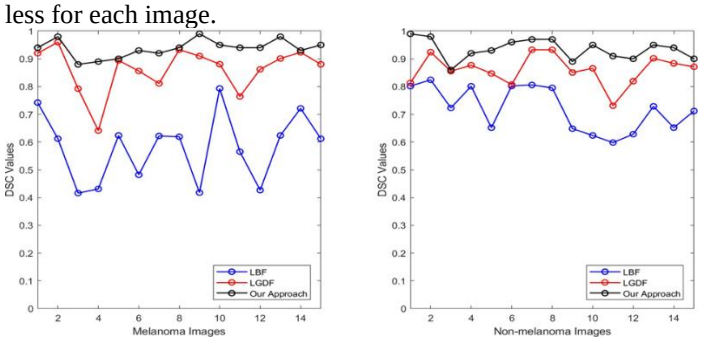

Figure 9: Graphical comparison of LGDF, LBF, and our approach's DSC value. The left compares fifteen melanoma photos, whereas the right compares fifteen non-melanoma scans.

Second, it works even with image lighting effects, which can drastically reduce segmentation accuracy. Using K-mean clustering to categorise and partition pixels into skin lesions and background, The lighting effect misclassifies background pixels within lesions when analysed alone, as seen in Figure 2(a). It is an intermediate aspect of our research. Our methodology yields results without misclassifications and higher segmentation accuracy, as illustrated in Figures 6(f) and 7(f). Table 1 shows higher Dice and Jaccard coefficients for our technique than LGDF and LBF.

Rough segmentation by k-mean clustering gives our LGDF model its initial outline. As illustrated in Figure 10, segmentation is done using k values from [2:9] to [2:11]. In k-mean clustering, increasing k has various effects on each image. We found from thorough investigation with different k values that increasing k after a certain limit in each image worsens segmentation outcomes. Sometimes background skin pixels are segregated as lesion pixels. The ideal k value for each image scenario is unpredictable and can only be determined visually. We found Segmentation findings are appropriate for k = 2, but when skin pixels merge with lesion pixels, segmentation results worsen.

As k in k-mean clustering increases, different lesion hues become clusters. Some lesion shade intensities match the backdrop, or skin intensity pixels. Lesion-skin intensity matches create empty spaces that can be filled with morphological operations. The k-mean clustering utilized here segments lesions, not classifies lesion hues. Most often, k = 2 is best for extracting the lesion's outer perimeter. We increase segmentation outcomes if holes from pixels inside a lesion match a skin lesion or if illumination brightens center pixels utilizing morphological techniques. If matching lesion pixels with skin are at the boundary or there is a little intensity difference, segmentation results are tough to improve. A big structuring element radius improved this problem in our technique.

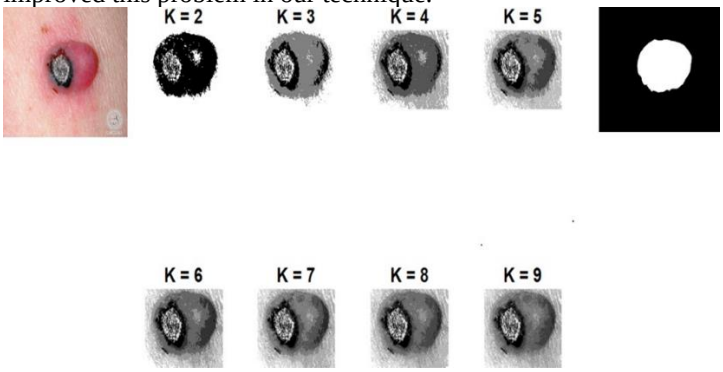

Figure 10: Example demonstrates k-mean clustering results for varied k values.

The disc covers more pixels at the lesion boundary and removes fewer holes than the structuring element. With a reduced radius, lesion holes may not fill entirely. A big radius is ideal for both huge holes after k-mean clustering and merged lesion and skin pixels at the boundary. If k-mean clustering results improve with a higher k parameter, it compensates for loss when k=2. The structural element radius is likewise limited. Figure 12 shows that increasing the radius beyond a certain limit merges incorrect pixels, reducing segmentation quality. We utilized k = 2 and a structuring element of radius 10 for rough segmentation based on these results.

For dermoscopy picture segmentation using JI and DSC metrics, various methods have been presented. Our method exceeds theirs by much. Similar to the Artificial Bee Colony (ABC) Algorithm in [44], the suggested method is applied to a DermIS data set with melanoma images. The average DSC and JI values are 0.9173 and 0.8356, compared to our 0.9373 and 0.9018. Similarly, an active contour-based segmentation approach [45] found an average DSC value of 0.8017 for PH2, a dataset of nevus and melanoma skin pictures. These two skin image segmentation methods are cutting-edge. Many other methods with similar outcomes and measurement values are available [46], [25]. We have an advantage over them due to this approach results.

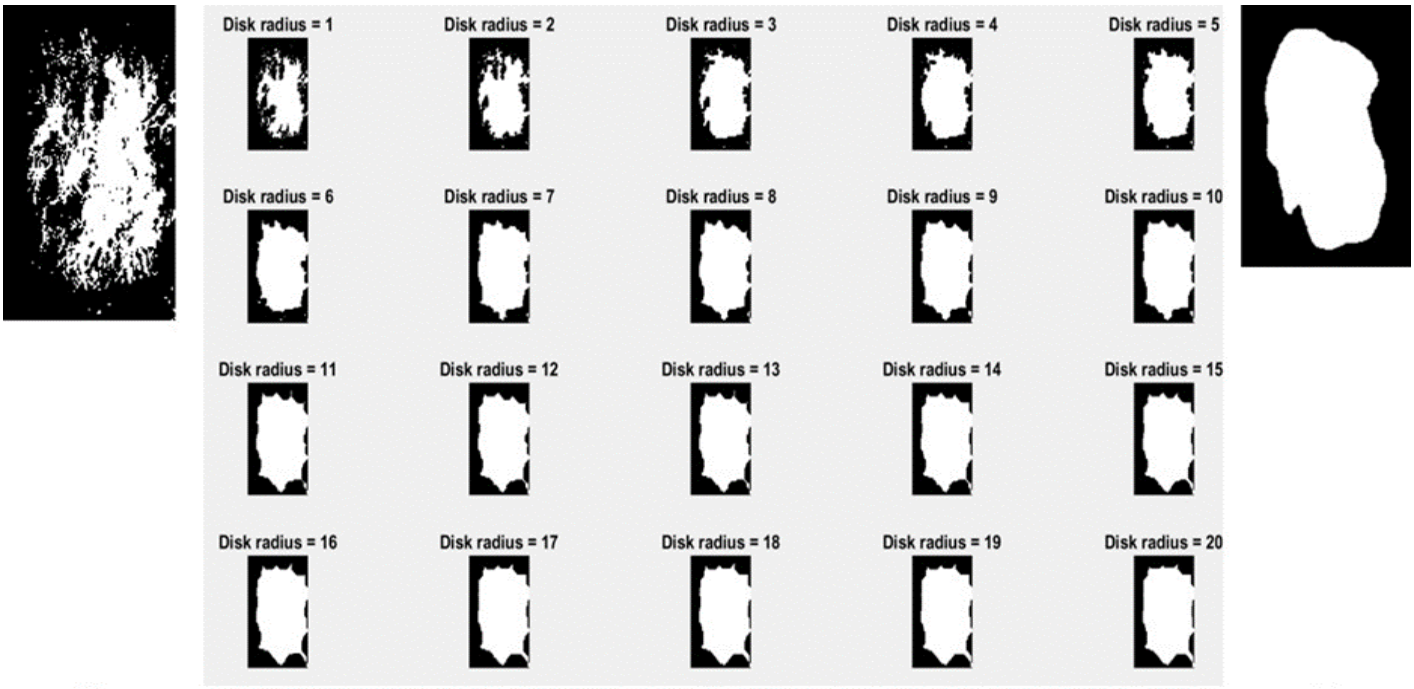

Figure 11: Example shows results for different sizes of the disk and structuring element.

VI. Conclusion

The purpose of this research is to present a novel approach that aims to reduce the computational burden, the dependence on precise initial contour placement within the Region of Interest (ROI), and the requirement for parameter adjustment across a variety of experiments that are inherent in the Local Gaussian Distribution Fitting (LGDF) model. A number of preprocessing processes are included in our methodology. These procedures include the extraction of the region of interest (ROI), which is then followed by the use of k-means clustering in order to create an initial segmentation of the lesion inside the ROI. Following the first segmentation of the region, subsequent morphological procedures are carried out in order to fill in any gaps or abnormalities that may have been present. A contour is then determined based on the border of the rough segmentation, which serves as the initial contour for the LGDF model. This contour is an initial contour.

The strategy that we have developed is intended to simplify the segmentation procedure and lessen the amount of computational complexity that is associated with the LGDF model. The goal of this project is to improve the accuracy and efficiency of skin lesion segmentation by automating the initialization of the model and applying morphological refinement. A comparative analysis was performed against both the LGDF model and the Local Binary Fitting (LBF) model in order to demonstrate the effectiveness of our suggested methodology through experimental evaluation. The results indicate that our method performs better than these models in terms of the accuracy of segmentation and the efficiency with which it uses computational resources. In addition to highlighting the potential of our technology for clinical applications in dermatology, this superiority demonstrates that our method is effective in precisely outlining skin lesions.

The findings of this work make a contribution to the ongoing efforts that are being made to develop enhanced segmentation techniques for medical imaging applications, particularly in the field of skin cancer diagnosis and treatment planning. It is possible that future research endeavors will concentrate on further refining the approach that has been provided and expanding it to accommodate a wide variety of datasets and lesion characteristics. This will ultimately lead to an advancement in the state of the art in computer-aided diagnosis systems for dermatological applications.

Acknowledgment

This work is financially supported by the National Center of Big Data and Cloud Computer (NCBC), University of Engineering and Technology, Peshawar, under the auspices of the Higher Education Commission (HEC), Pakistan.

References

[1] U. Leiter and C. Garbe, "Epidemiology of melanoma and nonmelanoma skin cancer the role of sunlight," in Sunlight, vitamin D and skin cancer, pp. 89–103, Springer, 2008.

[2] F. Bray, J. Ferlay, I. Soerjomataram, R. L. Siegel, L. A. Torre, and A. Jemal, "Global cancer statistics 2018: Globocan estimates of incidence and mortality worldwide for 36 cancers in 185 countries," CA: a cancer journal for clinicians, vol. 68, no. 6, pp. 394–424, 2018.

[3] B. K. Armstrong and A. Kricker, "The epidemiology of uv induced skin cancer," Journal of photochemistry and photobiology B: Biology, vol. 63, no. 1-3, pp. 8–18, 2001.

[4] R. Prasad and S. K. Katiyar, "Crosstalk among uv-induced inflammatory mediators, dna damage and epigenetic regulators facilitates suppression of the immune system," Photochem- istry and photobiology, vol. 93, no. 4, pp. 930–936, 2017.

[5] P. Schmid-Saugeona, J. Guillodb, and J.-P. Thirana, "Towards a computer-aided diagnosis system for pigmented skin lesions," Computerized Medical Imaging and Graphics, vol. 27, no. 1, pp. 65–78, 2003.

[6] M. Emre Celebi, Q. Wen, S. Hwang, H. Iyatomi, and G. Schaefer, "Lesion border detec- tion in dermoscopy images using ensembles of thresholding methods," Skin Research and Technology, vol. 19, no. 1, pp. e252–e258, 2013.

[7] Do Hyun Chung and G. Sapiro, "Segmenting skin lesions with partial-differential-equations- based image processing algorithms," IEEE Transactions on Medical Imaging, vol. 19, pp. 763–767, July 2000.

[8] L. Xu, M. Jackowski, A. Goshtasby, D. Roseman, S. Bines, C. Yu, A. Dhawan, and A. Hunt- ley, "Segmentation of skin cancer images," Image and Vision Computing, vol. 17, no. 1, pp. 65–74, 1999.

[9] P. G. Cavalcanti, J. Scharcanski, and G. V. Baranoski, "A two-stage approach for discrimi- nating melanocytic skin lesions using standard cameras," Expert Systems with Applications, vol. 40, no. 10, pp. 4054–4064, 2013.

[10] M. Emre Celebi, H. A. Kingravi, H. Iyatomi, Y. Alp Aslandogan, W. V. Stoecker, R. H. Moss, J. M. Malters, J. M. Grichnik, A. A. Marghoob, H. S. Rabinovitz, et al., "Border detection in dermoscopy images using statistical region merging," Skin Research and Technology, vol. 14, no. 3, pp. 347–353, 2008.

[11] M. E. Celebi, Y. A. Aslandogan, and P. R. Bergstresser, "Unsupervised border detection of skin lesion images," in International Conference on Information Technology: Coding and Computing (ITCC'05)-Volume II, vol. 2, pp. 123–128, IEEE, 2005.

[12] B. Manjunath and Y. Deng, "Unsupervised segmentation of color-texture regions in images and video," 2001.

[13] A. S. Ashour, Y. Guo, E. Kucukkulahli, P. Erdogmus, and K. Polat, "A hybrid dermoscopy images segmentation approach based on neutrosophic clustering and histogram estimation," Applied Soft Computing, vol. 69, pp. 426–434, 2018.

[14] F. Gasparini and R. Schettini, "Skin segmentation using multiple thresholding," in Internet Imaging VII, vol. 6061, p. 60610F, International Society for Optics and Photonics, 2006.

[15] Q. Abbas, I. Fond´on, A. Sarmiento, and M. E. Celebi, "An improved segmentation method for non-melanoma skin lesions using active contour model," in International Conference Image Analysis and Recognition, pp. 193–200, Springer, 2014.

[16] M. Mete and N. M. Sirakov, "Lesion detection in demoscopy images with novel density-based and active contour approaches," in BMC bioinformatics, vol. 11, p. S23, BioMed Central, 2010.

[17] M. Kass, A. Witkin, and D. Terzopoulos, "Snakes: Active contour models," International journal of computer vision, vol. 1, no. 4, pp. 321–331, 1988.

[18] B. Erkol, R. H. Moss, R. Joe Stanley, W. V. Stoecker, and E. Hvatum, "Automatic lesion boundary detection in dermoscopy images using gradient vector flow snakes," Skin Research and Technology, vol. 11, no. 1, pp. 17–26, 2005.

[19] V. Caselles, R. Kimmel, and G. Sapiro, "Geodesic active contours," International journal of computer vision, vol. 22, no. 1, pp. 61–79, 1997.

[20] T. F. Chan and L. A. Vese, "Active contours without edges," IEEE Transactions on image processing, vol. 10, no. 2, pp. 266–277, 2001.

[21] D. Mumford and J. Shah, "Optimal approximations by piecewise smooth functions and associated variational problems," Communications on pure and applied mathematics, vol. 42, no. 5, pp. 577–685, 1989.

[22] L. A. Vese and T. F. Chan, "A multiphase level set framework for image segmentation using the mumford and shah model," International journal of computer vision, vol. 50, no. 3, pp. 271–293, 2002.

[23] L. Wang, L. He, A. Mishra, and C. Li, "Active contours driven by local gaussian distribution fitting energy," Signal Processing, vol. 89, no. 12, pp. 2435–2447, 2009.

[24] O. Ronneberger, P. Fischer, and T. Brox, "U-net: Convolutional networks for biomedical im- age segmentation," in International Conference on Medical image computing and computer- assisted intervention, pp. 234–241, Springer, 2015.

[25] S. Khalid, U. Jamil, K. Saleem, M. U. Akram, W. Manzoor, W. Ahmed, and A. Sohail, "Seg- mentation of skin lesion using cohen–daubechies–feauveau biorthogonal wavelet," Springer- Plus, vol. 5, no. 1, pp. 1–17, 2016.

[26] A. Cohen, I. Daubechies, and J.-C. Feauveau, "Biorthogonal bases of compactly supported wavelets," Communications on pure and applied mathematics, vol. 45, no. 5, pp. 485–560, 1992.

[27] S. H. SALIH and S. AL-RAHEYM, "Comparison of skin lesion image between segmentation algorithms," Journal of Theoretical and Applied Information Technology, vol. 96, no. 18, 2018.

[28] M. Silveira, J. C. Nascimento, J. S. Marques, A. R. S. Marcal, T. Mendonca, S. Yamauchi, J. Maeda, and J. Rozeira, "Comparison of segmentation methods for melanoma diagnosis in dermoscopy images," IEEE Journal of Selected Topics in Signal Processing, vol. 3, pp. 35–45, Feb 2009.

[29] A. Pennisi, D. D. Bloisi, D. Nardi, A. R. Giampetruzzi, C. Mondino, and A. Facchiano, "Skin lesion image segmentation using delaunay triangulation for melanoma detection," Comput- erized Medical Imaging and Graphics, vol. 52, pp. 89–103, 2016.

[30] I. Zaqout, "Diagnosis of skin lesions based on dermoscopic images using image processing techniques," in Pattern Recognition-Selected Methods and Applications, IntechOpen, 2019.

[31] C. Barata, M. Ruela, M. Francisco, T. Mendon¸ca, and J. S. Marques, "Two systems for the detection of melanomas in dermoscopy images using texture and color features," IEEE Systems Journal, vol. 8, no. 3, pp. 965–979, 2013.

[32] R. Kasmi, K. Mokrani, R. Rader, J. Cole, and W. Stoecker, "Biologically inspired skin lesion segmentation using a geodesic active contour technique," Skin Research and Technology, vol. 22, no. 2, pp. 208–222, 2016.

[33] J. A. Hartigan and M. A. Wong, "Algorithm as 136: A k-means clustering algorithm," Journal of the Royal Statistical Society. Series C (Applied Statistics), vol. 28, no. 1, pp. 100– 108, 1979.

[34] H. Ng, S. Ong, K. Foong, P. Goh, and W. Nowinski, "Medical image segmentation using k-means clustering and improved watershed algorithm," in 2006 IEEE southwest symposium on image analysis and interpretation, pp. 61–65, IEEE, 2006.

[35] N. Dhanachandra, K. Manglem, and Y. J. Chanu, "Image segmentation using k-means clus- tering algorithm and subtractive clustering algorithm," Procedia Computer Science, vol. 54, pp. 764–771, 2015.

[36] P. Soille, Morphological image analysis: principles and applications. Springer Science & Business Media, 2013.

[37] R. [van den Boomgaard] and R. [van Balen], "Methods for fast morphological image trans- forms using bitmapped binary images," CVGIP: Graphical Models and Image Processing, vol. 54, no. 3, pp. 252 – 258, 1992.

[38] C. Li, R. Huang, Z. Ding, C. Gatenby, D. Metaxas, and J. Gore, "A variational level set approach to segmentation and bias correction of images with intensity inhomogeneity," in International Conference on Medical Image Computing and Computer-Assisted Intervention, pp. 1083–1091, Springer, 2008.

[39] C. Li, C. Xu, C. Gui, and M. Fox, "Distance regularized level set evolution and its application to image segmentation," Image Processing, IEEE Transactions on, vol. 19, pp. 3243 – 3254, 01 2011.

[40] T. Brox, From pixels to regions: partial differential equations in image analysis. PhD thesis, Faculty of Mathematics and Computer Science, Saarland University, Germany, April 2005.

[41] T. Sørensen, T. Sørensen, T. Sørensen, T. SORENSEN, T. Sorensen, T. Sorensen, and T. Biering-Sørensen, "A method of establishing groups of equal amplitude in plant sociology based on similarity of species content and its application to analyses of the vegetation on danish commons," 1948. P. Jaccard, " 'E comparative study of the floral distribution in a portion of the alps and the jura," vol. 37.

[42] C. Li, C.-Y. Kao, J. C. Gore, and Z. Ding, "Implicit active contours driven by local binary fitting energy," in 2007 IEEE Conference on Computer Vision and Pattern Recognition, pp. 1–7, IEEE, 2007.

[43] M. Aljanabi, Y. E. O¨ zok, J. Rahebi, and A. S. Abdullah, "Skin lesion segmentation method for dermoscopy images using artificial bee colony algorithm," Symmetry, vol. 10, no. 8, p. 347, 2018.

[44] F. Riaz, S. Naeem, R. Nawaz, and M. Coimbra, "Active contours based segmentation and lesion periphery analysis for characterization of skin lesions in dermoscopy images," IEEE journal of biomedical and health informatics, vol. 23, no. 2, pp. 489–500, 2018.

[45] M. Bayraktar, S. Kockara, T. Halic, M. Mete, H. K. Wong, and K. Iqbal, "Local edge- enhanced active contour for accurate skin lesion border detection," BMC bioinformatics, vol. 20, no. 2, p. 91, 2019.

AUTHORS

First Author – Noor Badshah, Department of Basic Sciences, University of Engineering and Technology Peshawar, 25000, Pakistan.
Second Author – Nasru Minallah, Department of Computer Systems Engineering, University of Engineering and Technology Peshawar, 25000, Pakistan.
Third Author – Muniba Ashfaq, Department of Computer Systems Engineering, University of Engineering and Technology Peshawar, 25000, Pakistan.
Fourth Author – Muhammad Abeer Irfan, Department of Computer Systems Engineering, University of Engineering and Technology Peshawar, 25000, Pakistan.
Fifth Author – Asif Ahmad, Department of Basic Sciences, University of Engineering and Technology Peshawar, 25000, Pakistan.
Sixth Author – Mahmood Ul Hassan, Department of Basic Sciences, University of Engineering and Technology Peshawar, 25000, Pakistan.
Seven Author – Zain Anwer Memon, Department of Electronics Engineering, University of Sindh, Jamshoro, 76080, Pakistan.

Correspondence Author – **Muhammad Abeer Irfan,** Department of Computer Systems Engineering, University of Engineering and Technology Peshawar, 25000, Pakistan.